Gasque Albalate, M.; González Altozano, P.; Maurer, D.; Moncho Esteve, IJ.; Gutiérrez-Colomer, RP.; Palau-Salvador, G.; García-Mari, E. (2015). Study of the influence of inner lining material on thermal stratification in a hot water storage tank. Applied Thermal Engineering. 75:344-356. doi:10.1016/j.applthermaleng.2014.10.040.

STUDY OF THE INFLUENCE OF INNER LINING MATERIAL ON THERMAL STRATIFICATION IN A HOT WATER STORAGE TANK

María Gasque[1], Pablo González-Altozano[2], Daniel Maurer[2], Ignacio José Moncho-Esteve[2], Rosa Penélope Gutiérrez-Colomer[2], Guillermo Palau-Salvador[2], Eugenio García-Marí[2].

Universitat Politècnica de València. Camino de Vera s/n. 46022 Valencia (Spain)

[1] Dept. Física Aplicada. e-mail: mgasque@fis.upv.es

[2] Dept. Ingeniería Rural y Agroalimentaria

ABSTRACT

The present study has analyzed the influence of thermal conductivity of the inner lining material on the stratification process in a hot water tank during thermal charge and the later standby period. This analysis has been carried out numerically by a three-dimensional Computational Fluid Dynamics (CFD) model. Experimental measurements of temperature profiles are used to select and verificate the model, and to later validate CFD simulations. With the validated model, temperature over time at several heights, temperature profiles, velocity contours, water streamtraces and temperature contours, are studied and compared for three different inner lining materials. The obtained results confirm that a weak conducting lining material favours energy storage in the tank and the thermal stratification of water during charge and subsequent standby period. The effect of the inner lining material on the energy accumulated in water and on the moment of energy (stratification) is potentially enhanced when the material's thermal conductivity diminishes. The use of insulating paints as inner lining for water storage tanks could be a possible solution to be studied and subsequently adopted in practice to improve the efficient use of energy in stored water. The analysis

techniques employed prove most useful and enable the results to be compared and presented in a novel way.

Keywords: Water stratification, Thermal energy storage, Inner lining material, CFD

1. INTRODUCTION AND OBJECTIVES

Thermal stratification in hot water storage tanks, its improvement, preservation and degradation, have been the subject of numerous research works in recent years [1,2]. Many studies about flow in these energy storage devices have concluded that the effectiveness of thermal storage depends on many factors, including temperature ranges, flow rate, inlet/outlet diffuser, aspect ratio, thickness insulation, or tank wall thermal conductivity and thickness, among others [1-3].

In this sense, the influence of wall conduction on thermocline degradation processes has been investigated both experimentally and numerically and it has been concluded that heat loss through the conductive walls and insulation have a considerable effect on thermal stratification decay in storage tanks [4,5]. In order to diminish the axial heat conduction effect and to preserve or improve stratification, several studies have proposed insulating the inner wall surface by placing insulation material or any low thermal conductivity material compatible with stored fluid [6-9].

The aforementioned previous research works have been carried out with very basic one or two-dimensional numerical models, or with experiments that provide much less information and data than current ones can obtain. In numerical studies, one-dimensional models cannot describe the flow structure within the tank in detail, especially under high flow rate and complex structure conditions [1]. Moreover, even though current numerical studies are mainly two-dimensional, three-dimensional models provide more accurate and realistic results [10,11]. Accordingly, Computational Fluid Dynamics (CFD) modeling is a useful tool to analyze three-dimensional flows. Indeed, many references can be found in recent research works which used CFD to investigate thermal stratification within water storage tank [1]. The great majority of these studies have been focussed on the effect of tank design parameters such as the diffuser configuration [12] or aspect ratios and operating conditions [10,11,13-15].

Nevertheless, to our knowledge, no work analizes the effect of storage tank wall material on the degradation of thermal energy by using CFD.

This paper presents a numerical study of transient three-dimensional heat transfer and flow characteristics in a hot water storage tank by means of CFD for the purpose of improving thermal stratification and, consequently, overall system efficiency. The CFD model employed and validated in this paper focuses on the effects of inner tank wall lining material on the level, evolution and stability of thermal stratification over time.

In order to determine the influence of lining material, a comparative study of how temperature evolves at various heights is carried out. Three materials with very different thermal conductivities have been considered: steel, expanded polystyrene, and poly methyl methacrylate. Temperature profiles, thermoclines, velocity contours and water streamtraces, as well as the temperature contours in water and through tank walls are represented and analyzed at different times. Likewise, the increment of energy and the moment of energy are calculated. The process is studied during the charge period (full thermal charge and partial charge), and also during the post-charge standby period.

2. MATERIALS AND METHODOLOGY

2.1. EXPERIMENTAL SETUP AND INSTRUMENTATION

The tank prototype for hot water storage used in this study consisted in a prismatic vessel, constructed with 20 mm thick poly methyl methacrylate plates (PMMA). The inner dimensions of the vessel were 600x280x100mm, with a water capacity of 16.8 L. The exterior was covered with a layer of insulating material: flexible elastomeric foam insulation, synthetic rubber-based (thermal conductivity, k=0.036 $W \cdot K^{-1} \cdot m^{-1}$), 20 mm thick. The water inlet and outlets were located at the top and bottom of the tank,. They were equipped with diffusers consisting of two parallel plates since it has been shown that these devices improve the

performance of thermal storage tanks by restraining mixing induced by water inflow [12,16-18]. Dimensions and constructive features of this prototype were conditioned because the tank was built with a dual purpose: on the one hand the mathematical modeling with CFD presented in this work, validated against experimental trials; and on the other hand, the determination and characterization of the flow velocity field applying the Particle Tracking Velocimetry (PTV) technique. PTV is a useful tool to complement numerical flow simulation results derived from approaches based on CFD. The results deduced from the analysis of the hydrodynamic performance of this hot water storage tank using PTV are not presented in this work.

Figure 1 provides a schematic view of the tank. To record the water temperature inside the tank, two probes, each of 8 type T (class 1) thermocouples, were placed uniformly along the tank height. Two other thermocouples were used to record the water inlet and outlet temperatures in the tank during the charge period. After calibrating the thermocouples, the accuracy of the temperature measurements was considered to be ±0.1 K. Water flow was measured at the tank outlet by an electromagnetic flowmeter (Siemens Sitrans FM MAGFLOW MAG5000 DN3 error < 0.5%). The signal of all the sensors was recorded using the CompactDAQ 9178 data acquisition system of National Instruments (NI), with an NI-9213 module (16-ch thermocouples, 24 bits) for thermocouple signal conditioning and acquisition, and an NI-9208 module (16-ch mA, 24 bits) for flowmeter signal acquisition. Readings were taken every 10 seconds and were transferred to a personal computer, where they were processed by Labview 2010 (NI). Apart from the elements described, the experimental setup included two extra constant level tanks, one thermostatted at a temperature of 293 K and the other at 324 K. This configuration was used to ensure a constant temperature and flow in the tank inlet while the experiment was underway.

Two experiments, A and B, with the characteristic parameters summarized in Table 1, were carried out. Experiment A allowed model selection, verification of the mesh and validation, whereas experiment B was used only to validate the model (simulation cases S-VA and S-VB).

Both experiments were conducted in the tank with an initial internal uniform water temperature of about 293 K. A constant water flow (6 and 15 $mL \cdot s^{-1}$) was injected from the tank thermostatted to 324 K. Simultaneously, an equivalent water flow was extracted through the bottom tank outlets. The duration of the charge cycle in both trials allowed the stored water to be completely renewed (107% and 117%). After finishing the charge period, the tank inlet and outlets were closed, and the signal provided by the thermocouples continued to be recorded during 7 h (25,200 s), and allowed the validation of the CFD model during the standby period.

2.2. NUMERICAL ANALYSIS

The thermal stratification process during the charge and the subsequent standby period was studied by a Computational Fluid Dynamics (CFD) model with the software STAR-CCM+ Ver. 5.04.006 of CD-adapco. The computational scheme solves the incompressible Navier-Stokes equations in integral form for continuity and momentum:

$$\frac{d}{dt}\int_V \rho \, dV + \oint_A \rho \, v \cdot da = 0 \tag{1}$$

$$\frac{d}{dt}\int_V \rho \, v \, dV + \oint_A \rho \, v \wedge v \cdot da = -\oint_A p \, I \cdot da + \oint_A [T] \cdot da + \oint_V f_g dV \tag{2}$$

where ρ is density; v is velocity; p is pressure; [T] is the viscous stress tensor; a is the face area vector; V is cell volume; A is cell area; I is the identity matrix; and f_g represents the effects of buoyancy.

Water density was calculated according to temperature (273-373 K), as follows:

$\rho = 740.8747 + 1.96765 \times T - 0.003720 \times T^2$

For all the studied cases, the realizable k-ε model turbulent approach [19] was used. However the influence of the turbulence in the flow was rather small. Comparisons with laminar flow simulations were obtained and no significative differences were found except in the upper part of the tank where the turbulent model predicts more accurately the stratification process. For this reason, the results presented in this paper are those obtained with a turbulent closure.

A second-order segregated fluid temperature model was employed. The segregated fluid temperature model solves the total energy equation with temperature as the independent variable, as follows:

$$\frac{d}{dt}\int_V \rho E\, dV + \oint_A [\rho H v]\cdot da = -\oint_A q''\cdot da + \oint_A [T]\cdot v\, da + \int_V f\cdot v\, dV \qquad (3)$$

where E is the total energy; H is the total enthalpy; q'' is the heat flux vector; and f is the body force vector representing buoyancy effects in this case. Total energy (E) is related to the total enthalpy (H) by: $E = H - p/\rho$, where: $H = h + |v|^2/2$, and $h = c_p T$, being c_P the specific heat of water and T, temperature.

2.2.1.***Computational domain, grid and boundary conditions***

The CFD model was performed for experiments A (simulation S-VA) and B (simulation S-VB), as previously mentioned.

In the water body, a structured mesh was defined. In order to improve the model agreement and to resolve better the details around the inlet and outlet sections, further grid points were added mainly in these regions. Several grids were tested in order to check the grid dependency of the solution. Characteristics of three of the grids tested (A-B-C) are shown in Table 2. The grids are finer near the walls and the maximum grid size variation between cells is kept to an increase of 7%. The mesh finally selected was grid B. This selection was done taking into account the results between simulations with the three meshes and the grid convergence

index, GCI [20]. The maximun GCI was 0.74% between A and B grids, and 0.20% between B and C ones.

Time steps of 1 second and a first-order upwind convection scheme with an implicit solver were selected. The time step influence on the simulation was verified by using time steps between 0.5 and 10 seconds. Not significant differences were found between 1 and 0.5 seconds.

Regarding the boundary conditions, the inlet was defined as velocity inlet with a value of 0.1184 $m \cdot s^{-1}$ ($Q=6.0\ mL \cdot s^{-1}$) in simulation S-VA, and of 0.2990 $m \cdot s^{-1}$ ($Q=15.0\ mL \cdot s^{-1}$) in simulation S-VB. It was assumed that the initial temperature of the PMMA vessel was the same as the initial interior water temperature. The incoming water temperature was set as indicated in Table 1. The two outlet boundary conditions were considered with an equal outflow (50% of inlet flow each one). All the other boundaries were fixed as smooth walls. Wall treatment was done with a model for y+ larger than 30 and the boundary layer was resolved in the other cases [21].

In order to simulate the heat transport within the PMMA wall, an unstructured grid was defined for the PMMA vessel. The reference values for the polyhedral mesher were set for a minimum surface size of 0.5 mm and a surface growth rate of 1.5. Thus, the PMMA vessel mesh was made up of 27,725 cells.

In all the cases considered in this study, energy transport was taken into account on the contact surfaces between the vessel and water, and it was performed with a contact interface condition (STAR-CCM+ Ver. 5.04.006 of CD-adapco). The energy transport or losses produced by diffusers or pipes were neglected. Energy losses from the vessel to the surroundings were modeled with a constant convective heat transfer coefficient $h_c = 1.75\ W \cdot K^{-1} \cdot m^{-2}$, which was experimentally determined with an ambient temperature of 294.82 K, considered to be the ambient temperature in all the CFD simulations.

The model was supplied with the following constant values of viscosity (μ), specific heat (c_P) and thermal conductivity (k) as basic inputs for the water region: μ_{H2O} = 8.8871 x 10^{-4} kg·m^{-1}·s^{-1}, $c_{P(H2O)}$ = 4,181.72 J·kg^{-1}·K^{-1} and $k_{(H2O)}$ = 0.620271 W·m^{-1}·K^{-1}. The physical characteristics defined for the PMMA vessel were $c_{P(PMMA)}$ = 1,420 J·kg^{-1}·K^{-1}, $k_{(PMMA)}$ = 0.16 W·m^{-1}·K^{-1} and $\rho_{(PMMA)}$ = 1,188 kg·m^{-3}.

To check the suitability of the CFD model and to validate it, the evolution of temperature over time was studied at the position of the thermocouples during both the charge cycle and the standby period. Model predictions were compared with the measured experimental temperatures, and the Root Mean Squared Error (RMSE, K) was calculated to introduce a relative measure of the error as follows:

$$\mathrm{RMSE} = \left(\frac{1}{n} \cdot \sum_{i=1}^{n} \left(x_i - \hat{x}_i \right)^2 \right)^{0.5}$$

where x_i and $\hat{x}_i$ are the experimental and estimated values of temperature, and n is the number of observations.

The mesh used for the water domain and the tank wall of PMMA, and a detail of the mesh of the inlet/outlet diffusers as well as their dimensions, are included in Fig. 2.

2.2.2. Effect of inner tank wall lining material

The validated CFD model was used to study the influence of the inner tank wall lining material on the stratification process during the charge cycle and the standby period. Three inner lining materials with very distinct thermal conductivities (high, intermediate and low) were considered. As steel is a very commonly used material in the manufacturing of hot water storage tanks, it was decided to select it as the high thermal conducting material ($k_{(STEEL)}$ = 16.26 W·m^{-1}·K^{-1}). Expanded polystyrene (EPS) was selected as a weak conducting material ($k_{(EPS)}$ = 0.034 W·m^{-1}·K^{-1}), and PMMA as an intermediate conducting material ($k_{(PMMA)}$ = 0.16 W·m^{-1}·K^{-1}). These cases were named S-STEEL, S-EPS and S-PMMA. S-PMMA corresponded to simulation

S-VA, used to validate the CFD model. An adiabatic process (S-AD), was also considered as a control case given that in such a process, transmission by conduction through tank walls does not occur and the transport of the heat inside the tank is due only to the temperature gradient and flow movement. The various simulations (Table 3) were performed with the same values as the characteristic parameters of trial A ($Q = 6.0$ mL·s^{-1}, $T_{inlet} = 324.08$ K, $T_{ini} = 293.08$ K).

Two charge durations were considered for each case, a full charge and a partial one. The full charge corresponded to 107.2% of total tank volume (3,022 s), while the partial charge corresponded to 63.8% (1,800 s). After each charge period, flow was set to zero, and the simulation continued for 7 h after starting (25,200 s). Ambient temperature was fixed in all the simulations at 294.82 K, the same as in trial A.

The physical values (c_P and ρ) for the inner STEEL and EPS layers were $c_{P(STEEL)} = 502.1$ J·kg^{-1}·K^{-1}, $\rho_{(STEEL)} = 8{,}027.2$ kg·m^{-3}, and $c_{P(EPS)} = 1{,}500$ J·kg^{-1}·K^{-1}, $\rho_{(EPS)} = 20$ kg·m^{-3}. The meshing of these regions was performed with triangular prisms (Fig. 2). A minimum surface size of 7.5 mm and a surface growth rate of 1.3 for two thin layers were used. Thus a mesh with 29,443 cells was obtained. The new region was connected with the water and the PMMA regions with in-place interfaces.

In the adiabatic model proposed as the control, the vessel region was deleted and all the wall boundaries were set to adiabatic.

2.3. Procedure to analyse the results

Different analysis procedures were employed to study the influence of lining materials on thermal stratification. The evolution of water temperature at various tank heights corresponding to the thermocouple locations was compared during both, the thermal charge (full and partial) and the post-charge standby period. Afterwards the influence of the lining material was also studied based on several parameters, some of which are described below.

The increment of thermal energy stored, ΔE (J), was established at different times during both the partial charge and the standby period in the water and through the tank walls by estimating the energy values from flow and temperature [22]. The increment of energy in the tank at instant t=tj, as compared to the initial instant, was calculated by a field function user defined in STARCCM+ as the sum of the increment of energy in all the cells into which the domain was divided:

$$\Delta E(t_j) = \sum_{i=1}^{n} V_i \cdot \left[\left(\rho_i \cdot c_p \cdot T_{i,j} \right) - \left(\rho_{i\_ini} \cdot c_p \cdot T_{ini} \right) \right] \quad (4)$$

where n is the number of cells; V_i (L) the volume of cell i; $T_{i,j}$ (K) the temperature of cell i at instant t_j; ρ_i (kg·L^{-1}) the density at $T_{i,j}$; c_P (J·kg^{-1}·K^{-1}) the specific heat; ρ_{i_ini} (kg·L^{-1}) the initial density; and T_{ini} (K) the initial temperature (293.08 K).

To check the thermodynamic coherence of the CFD model, ΔE determined by Eq. (4), was applied to the adiabatic simulation (S-AD) performed as a control (ΔE_{ad_sim}), and was compared with the ΔE obtained theoretically (ΔE_{ad_theo}) in an adiabatic process. This ΔE_{ad_theo} can be determined at instant t_j during the charge cycle by considering that no water mixing or heat losses through walls had occurred, from Eq. (5):

$$\Delta E_{ad\_theo}(t_j) = Q \cdot t_j \cdot [(\rho_{inlet} \cdot c_P \cdot T_{inlet}) - (\rho_{ini} \cdot c_P \cdot T_{ini})] \quad (5)$$

where Q (mL·s^{-1}) is the flow; t_j (s) is the charge time; ρ_{inlet} (kg·L^{-1}) the density at T_{inlet}; and ρ_{ini} (kg·L^{-1}) the density at T_{ini}.

Another parameter determined in this work is the moment of energy ME (J·m) [23], a useful index for comparing the ability to promote and maintain stratification during the charge and standby period if the compared cases have the same water geometry. ME is greater the higher the temperature is and the further away it is from the storage tank base. Therefore, a higher degree of stratification leads to higher ME values. So this parameter proves most suitable for this analysis.

ME was determined at each instant t_j during the partial charge, and also during the standby period, by means of a field function user defined of STAR CCM+ and by summing the ME in each cell into which the domain was divided:

$$ME\left(t_j\right) = \sum_{i=1}^{n} V_i \cdot \rho_i \cdot c_p \cdot T_{i,j} \cdot d_i \quad (6)$$

where d_i (m) is the distance from the center of cell i to the tank base.

The evolution of accumulated ΔE in the water and in the tank walls, and ME in the water were analysed with the three lining materials during the partial charge and the standby period. Both parameters were expressed as a percentage in relation to the adiabatic process.

The graphic representation of the temperature profiles, temperature contours in water and through tank walls, velocity profiles and water streamtraces, have also been analyzed at different times to compare stratification efficiency among the various inner tank wall lining materials.

3. RESULTS AND DISCUSSION

3.1. Experimental validation of the CFD model

Figure 3 shows the evolution of the water temperature in the thermocouples locations of the central probe (TC) during the full charge (3,022 s, 107% of total volume), and part of the subsequent standby period, until 7,200 s (the whole of the standby period lasted until 25,200 s). This Figure depicts both the experimentally determined temperature data (trial A) and estimated from the CFD model (S-VA).

During the charge, the simulation matched the experimental results quite well. It is observed how the temperature at each thermocouple location rose almost at the same time with a similar trend in both the experiment and simulation (the shape and slope of the curves and the maximum temperature reached were similar). The maximum time lag between the simulation results and the experiment was 44.60 seconds at the first thermocouple, with an

average time lag during the charge of 20.16 s. Maximum temperature differences were 6.37 K (RMSE of 1.3070 K) with an average of 0.35 K (RMSE of 0.7433 K).

During the standby period, also a good correspondence between the values of experimental temperatures and the simulation was found. The larger differences were observed toward the end of the standby time in the thermocouple situated at a lower height (1.71 K), probably because the model did not consider heat losses from poorly isolated valves and connecting pipes located at the bottom of the tank.

The validation of the simulations with trial B also led to a close correspondence between the experimental and numerical values in a similar way to that obtained with trial A. The maximum difference during the charge between the estimated and the experimental values was 23.40 seconds at the lower TC, with a mean difference of 4 seconds. Maximum temperature differences were 2.42 K (RMSE of 0.5557 K) with an average of 0.24 K (RMSE of 0.4987 K). Although minor differences were noted in the shape and slope of the curves between the experimental and simulation results, these differences were always in the same direction and showed no great magnitude. During the standby time, the simulation S-VB results were also similar and very close to those obtained with trial B.

The temperature values estimated with the model and those obtained in the experimental trials with the lateral thermocouples (TL) gave similar results to those obtained when using the values given by the central thermocouples (TC). Thus, the model reproduced well the water temperature profile at both the vertical and horizontal planes.

3.2. Effect of inner tank wall lining material on thermal stratification

3.2.1. Time dependent temperature profiles

Figure 4 illustrates the evolution of temperature at the TC locations during the thermal full charge (107.2%) of those simulations carried out to compare the influence of the inner

lining materials (S-STEEL, S-PMMA and S-EPS) on the stratification process. S-PMMA corresponds to simulation S-VA, used to validate the CFD model.

With the three materials, the temperature front reached each TC location practically at the same time given that the input flow was the same in all cases (6 $mL \cdot s^{-1}$). Nevertheless, temperature rose more quickly when the lining material conductivity was lower, as the different slope of the curves indicates. The maximum temperature reached by the TC located higher up was similar in all three cases. However, the lower the position of the thermocouples, the more marked the differences in both the maximum temperature accomplished and the profile slope. These results indicate a higher and a lower degree of mixing for the STEEL and the EPS lining. The differences in temperatures among the three materials found during the charge time remained throughout the standby period (results not shown).

The evolution of water temperature during the process with a partial charge (63.8%, Fig. 5) differed from that with a full charge. At the end of the partial charge, only the top of the tank was heated, whereas the bottom remained at the initial lower temperature. Thus, during the standby period after the partial charge, the temperature in the heated area started to drop, while it rose in the cooler tank area. This increase was due to thermal diffusion and convection processes in the water and conduction through the walls, and not to the heat exchange outward the tank given the similarity of its temperature to the ambient temperature.

In the case with more conductive lining (STEEL) the temperature increased at the bottom of the tank and decreased at the top of the tank (TC3 and TC4) to a greater extent than with the other materials. This confirms that a higher degree of stratification was maintained when the material was more insulating (EPS).

3.2.2. Increment of energy accumulated in the tank

The error in determining the increment of accumulated energy from the CFD simulations (ΔEad_sim), related to that determined theoretically (ΔEad_theo), was relatively constant and always below 0.14%, which is lower than that reported by Shyu and Hsieh [7].

The increment of energy accumulated in the water domain and in the tank wall (expressed as a percentage of accumulated energy in relation to that in the adiabatic process, S-AD) is shown in Fig. 6.

As expected, the insulating effect of EPS favoured the accumulation of energy in water to a greater extent than the other materials, with the greatest differences found for the lining with STEEL (between 6.2% and 5.1% during the charge, and between 5.3% and 2.9% during the standby period). The differences between the energy accumulated in water with EPS and PMMA were less marked (between 2.9% and 2.6% during the charge, and between 3.2% and 1.7% during the standby period). These results confirm that the lining materials offering worse thermal conductivity favoured not only the accumulation of energy during the charge, but also its maintenance in a significant amount during the subsequent standby period.

3.2.3. Moment of energy

The ME calculated for all materials with respect to the adiabatic model was progressively reduced throughout the process, and this reduction was greater especially during the charge period (Fig. 7). Therefore in the three cases under study, stratification got worse during the charge more quickly than during the standby period.

The ME values always remained higher the lower the inner lining conductivity was, although the differences found were minor.

The lower conductivity of EPS as compared to PMMA and STEEL improved ME. However, this effect was due to both the greater accumulated heat in the water given the insulating effect of EPS and the better stratification.

As observed in Fig. 8, the conductivity coefficient of material (k) revealed a power-type relationship with ΔE with a negative exponent ($\Delta E=a\cdot k^{-b}$). This indicates that the effect on energy accumulation became more marked as the conductivity of the lining material lowered. The k-ME relationship showed the same tendency (results not shown). Both relationships indicate that accumulated energy and stratification were particularly favoured with low conductivity materials.

3.2.4. Temperature contours and streamtraces

In the enlarged details of the tank wall depicted in Fig. 9, the evolution of the temperature contours in the symmetrical tank plane is represented at two times during the thermal full charge. The tank wall clearly remained colder in EPS than in the other two materials, which performed similarly. This effect was the direct result of the insulating capacity of EPS. Regarding the uniformity of temperature with height, the isothermal lines indicate that the brusquest changes in temperature took place in the areas nearer the wall and that they were more marked the higher the material's conductivity. The material's conductivity also affected the forward speed of the wall's temperature in relation to that of water's temperature.

Since the conductivity of the STEEL lining is higher, the surface that came into direct contact with hot water practically reached the same temperature transmitting heat toward the tank wall. In the case of EPS, the insulation buffered considerably the methacrylate wall heating.

Figure 10 provides the horizontal temperature profiles at different heights during the standby period at 3,600 s after the partial charge (63.8%). The water temperature was constant at the various heights and was consistent with the distribution of the temperatures for each material shown in Fig. 9. The temperature through the wall drastically dropped, and this reduction was more pronounced the lower the lining material's conductivity was.

Figure 11 shows the temperature contours and streamtraces at the end of the partial charge (1,800 s, 63.8%) in the four cases analyzed. Despite their minor importance, relatively symmetrical recirculations related to the injection from the inlet diffuser are seen at the top, more extended for S-AD than for the other cases. It is important to stress that the velocities were relatively low in all the studied cases, similar among S-STEEL, S-PMMA and S-EPS (0.0084 $m \cdot s^{-1}$ on average), and 13% greater in S-AD (0.0094 $m \cdot s^{-1}$). In the latter case, the process was more influenced by the convection processes due to the hot water flow in the tank inlet.

The greater velocities, which occurred in the area near the outlet, were similar with all three lining materials (-0.1571 $m \cdot s^{-1}$ on average), and were 15% greater than those in the adiabatic process (-0.1369 $m \cdot s^{-1}$). This can be explained because the water circulated homogeneously through the entire tank section in the S-AD case, whereas for the other three materials, streamtraces tended to concentrate in the central tank area, and particularly at the bottom of the tank.

Figure 12 depicts the temperature contours and streamtraces at the end of the standby period (25,200 s). In STEEL, PMMA and EPS, two zones marked by the characteristics of the fluid flow are seen: on the one hand, an upper zone, where the heat loss from the tank sides and thermal conduction through the wall cool down the water temperature close to wall creating a downward flow. Simultaneously, in the center of the tank, the water with higher temperatures flows upwards. On the other hand, a lower zone, in which the water close to the tank side walls heats up because of thermal conduction creating thereby an upward flow. At the same time, water flows downwards in the central part of this lower zone. Similar driven flows were described in [14]. For S-AD, this separation did not appear and mixing occurred in the entire tank volume, as shown by the numerous recirculations appearing throughout the domain. In this case, the magnitude of the velocity inside the tank was very low, with maximum values of 0.00047 $m \cdot s^{-1}$, which was 20% as compared to the mean maximum velocity

recorded in the other three cases (similar to each other and 0.00244 $m \cdot s^{-1}$ on average). At the end of standby period, the degree of thermal stratification was similar with PMMA and EPS and higher in both cases to that achieved with STEEL.

Figure 13 presents the streamtraces over the velocity contours at two times during the standby period after the partial charge (63.8%) obtained in the three lining materials. The temperature profiles are also included on the right at the same time instants. The downward flow is depicted in blue while the upward one is denoted in red. The change in colour distinguishes the two zones aforementioned when discussing Fig. 12: the lower cold zone (blue) and the upper hot and mixing zone (red). The water mixing between both these two zones was poor, as confirmed by the fact that the cold water temperature barely changed throughout the standby period. Similar results were obtained by other researchers [6,7] .

The separating line between both zones coincides with the lower part of the thermocline in the three cases throughout all the standby period. However, in the case of STEEL, the distance between the upper and lower zones is at a height (Z) of the tank with more temperature gradient than in the case of the other two materials tested.

Figure 14 includes the vertical velocity profiles of water at various tank heights at time t = 3,600 s during the standby period after a partial charge (63.8%). The greatest velocities took place in the hot and mixing zone of the tank. They were negative and of greater magnitude in the region in contact with the wall, and they abruptly rose and became positive in the vicinity of the wall, and remained more or less constant throughout the section. The higher velocities and the most abrupt changes took place in the upper area (z=0.5 m) and diminished with height (z=0.3 m). In the lower area (the cold zone of the tank), a change occurs in the flow behavior in the vicinity of the wall appearing ascending velocities (z=0.1 m). In the proximity of the shallowest tank area (z=0.05 m), these ascending velocities became increasingly higher. Such observations provide details of how flow behaved in the two zones set out in Fig. 13. It is

also noteworthy that the behaviour observed in the adiabatic case produced no variation in the zone close to the wall, with homogeneous velocities on the whole tank surface, except in the upper zone (z=0.5m) where certain variations emerged owing to the recirculations observed in Fig. 12 for this very case.

4. CONCLUSIONS

The influence of inner tank lining material on thermal stratification in a vertical prismatic hot water storage tank prototype has been investigated numerically by CFD. The process has been studied during the full and the partial charge cycles (107% and 64% of the total tank volume replaced), and during a standby period until 7 h, which was completed in both the charge cases. Three inner lining materials with very different thermal conductivities have been considered: steel, expanded polystyrene, and poly methyl methacrylate.

A three-dimensional CFD model has been selected, verificated and validated with experimental measurements. The correspondence between the experimental results and the model estimations has resulted excellent. The maximum temperature differences were 6.37 K (RMSE of 1.3070 K) with an average of 0.35 K (RMSE of 0.7433 K). Moreover, the error in determining the increment of accumulated energy from the results of the CFD model was less than 0.14%. Thus, the CFD model predicts the experimental results very accurately.

Evolution of the water temperature at different tank heights, increment of energy accumulated in the water and in tank walls, moment of energy in water, temperature profiles, and temperature and velocity contours, as well as streamtraces, have all been analyzed. All the results obtained indicate that a weak conducting material in contact with water, favours energy storage and stratification during the thermal charge and the post-charge standby period. Nevertheless, the effect is more marked during the thermal charge and is attenuated with storage time as the standby period advances. The effect of the inner tank lining material

on the energy accumulated in water and the moment of energy (stratification) is potentially enhanced when the material's thermal conductivity lowers. It is to be noted that high thermal conducting lining material (STEEL) promotes mixing due to thermal diffusion along the side wall and axial heat losses through the conducting metallic wall. When placing lining materials having low or intermediate thermal conductivity (EPS and PMMA), discharging efficiency improves with decreasing thermal diffusion and heat leak via the enclosure wall. Thus, thermal stratification improves with decreasing wall thermal conductivity for EPS, PMMA and STEEL in that order. The inner lining material of the storage tank wall is found to have little effect on thermal stratification during charging and standby period. Nevertheless, this effect should not be neglected as it is desirable that the maximum energy must be conserved in these kind of systems. Therefore, the use of insulating paints as inner lining for water storage tanks could be a possible solution to be studied and subsequently adopted in practice to improve the efficient use of energy in stored water.

The three-dimensional techniques utilized in the numerical modeling and in the data analysis are a very useful tool to assess the effects of the inner lining material on stratification. These techniques enable the results to be compared and presented in a novel manner that is easier to interpret than in former works.

5. ACKNOWLEDGMENTS

This research was supported by the *Plan Nacional de I+D+i del Ministerio de Ciencia e Innovación* (ENE2009-13376). The authors would like to thank L.H. Sanchis for his valuable and constructive suggestions during the planning and development of this research.

6. NOMENCLATURE

AD = adiabatic

CFD = Computational Fluid Dynamics

c_p = specific heat, $J \cdot kg^{-1} \cdot K^{-1}$

d_i = distance from the center of cell i to the tank base, m

EPS = expanded polystyrene

h_c = convective heat transfer coefficient, $W \cdot K^{-1} \cdot m^{-2}$

IM = insulating material (flexible elastomeric foam synthetic rubber-based)

k = thermal conductivity coefficient, $W \cdot K^{-1} \cdot m^{-1}$

ME = moment of energy, J·m

n = number of cells

PMMA = poly methyl methacrylate

Q = water flow injected and extracted during the charge, $mL \cdot s^{-1}$

RMSE = Root Mean Square Error, K

TC = thermocouples of central probe

TL = thermocouples of lateral probe

T_{amb} = ambient temperature, K

T_{ini} = mean initial water temperature, K

T_{inlet} = mean hot water inlet temperature during the charge, K

$T_{i,j}$ = temperature of cell i at instant t_j, K

t = time, s

V = cell volume, L

v = velocity, $m \cdot s^{-1}$

ΔE = increment of thermal energy stored, J

ΔE_{ad_sim} = increment of thermal energy stored in the adiabatic simulation case, J

ΔE_{ad_theo} = increment of thermal energy stored obtained theoretically considering an adiabatic process, J

μ = viscosity, $kg \cdot m^{-1} \cdot s^{-1}$

ρ = density, $kg \cdot m^{-3}$

7. REFERENCES

[1] Y. Han, R. Wang, Y. Dai, Thermal stratification within the water tank, Renewable and Sustainable Energy Reviews. 13 (5) (2009) 1014-1026.

[2] R. Shukla, K. Sumathy, P. Erickson, J. Gong, Recent advances in the solar water heating systems: A review, Renewable and Sustainable Energy Reviews. 19 (2013) 173-190.

[3] N. Gopalakrishnan, S.S. Murthy, Mixed convective flow and thermal stratification in hot water storage tanks during discharging mode, Applied Solar Energy. 45 (4) (2009) 254-261.

[4] M. Abdoly, D. Rapp, Theoretical and experimental studies of stratified thermocline storage of hot water, Energy Conversion and Management. 22 (3) (1982) 275-285.

[5] N. Al-Najem, Degradation of a stratified thermocline in a solar storage tank, International Journal of Energy Research. 17 (3) (1993) 183-191.

[6] S. Chaney, J. Humphrey, L. Month, A. Shah, Flow and heat transfer of a stably stratified fluid through an enclosure, Journal of Solar Energy Engineering. 106 (3) (1984) 261-270.

[7] R. Shyu, C. Hsieh, Unsteady natural convection in enclosures with stratified medium, Journal of Solar Energy Engineering. 109 (2) (1987) 127-133.

[8] R. Shyu, J. Lin, L. Fang, Thermal analysis of stratified storage tanks, Journal of Solar Energy Engineering. 111 (1) (1989) 54-61.

[9] S.S. Murthy, J. Nelson, T. Rao, Effect of wall conductivity on thermal stratification, Solar Energy. 49 (4) (1992) 273-277.

[10] S. Ievers, W. Lin, Numerical simulation of three-dimensional flow dynamics in a hot water storage tank, Applied Energy. 86 (12) (2009) 2604-2614.

[11] W. Yaïci, M. Ghorab, E. Entchev, S. Hayden, Three-dimensional unsteady CFD simulations of a thermal storage tank performance for optimum design, Applied Thermal Engineering. 60 (1-2) (2013) 152-163.

[12] J.D. Chung, S.H. Cho, C.S. Tae, H. Yoo, The effect of diffuser configuration on thermal stratification in a rectangular storage tank, Renewable Energy. 33 (10) (2008) 2236-2245.

[13] R. Consul, I. Rodrıguez, C. Perez-Segarra, M. Soria, Virtual prototyping of storage tanks by means of three-dimensional CFD and heat transfer numerical simulations, Solar Energy. 77 (2) (2004) 179-191.

[14] J. Fan, S. Furbo, Buoyancy driven flow in a hot water tank due to standby heat loss, Solar Energy. 86 (11) (2012) 3438-3449.

[15] J. Fan, S. Furbo, Thermal stratification in a hot water tank established by heat loss from the tank, Solar Energy. 86 (11) (2012) 3460-3469.

[16] A.J. Ghajar, Y.H. Zurigat, Numerical study of the effect of inlet geometry on stratification in thermal energy storage, Numerical Heat Transfer. 19 (1) (1991) 65-83.

[17] L.J. Shah, S. Furbo, Entrance effects in solar storage tanks, Solar Energy. 75 (4) (2003) 337-348.

[18] E. García-Marí, M. Gasque, R.P. Gutiérrez-Colomer, F. Ibáñez, P. González-Altozano, A new inlet device that enhances thermal stratification during charging in a hot water storage tank, Applied Thermal Engineering. 61 (2) (2013) 663-669.

[19] T. Shih, W.W. Liou, A. Shabbir, Z. Yang, J. Zhu, A new k-epsilon eddy viscosity model for high Reynolds number turbulent flows: Model development and validation, NASA-TM-106721. (1994).

[20] I.B. Celik, U. Ghia, P.J. Roache, C.J. Freitas, H. Coleman, P.E. Raad. Procedure for Estimation and Reporting of Uncertainty Due to Discretization in CFD Applications. Journal of Fluids Engineering. Transactions of the ASME 130(7) (2008) 0780011-0780014.

[21] CD-adapco Inc., Star-CCM+ Version 5.04.006. User guide. (2010).

[22] S. Alizadeh, An experimental and numerical study of thermal stratification in a horizontal cylindrical solar storage tank, Solar Energy. 66 (6) (1999) 409-421.

[23] J. Davidson, D. Adams, J. Miller, A coefficient to characterize mixing in solar water storage tanks, Journal of Solar Energy Engineering. 116 (2) (1994) 94-99.

LIST OF FIGURE CAPTIONS

Fig. 1. Schematic view of the tank with its dimensions (mm). The position of the central (TC) and lateral (TL) probes with 8 thermocouples each is also indicated.

Fig. 2. Left: details of the meshes in the different regions: water, STEEL/PMMA/EPS, and PMMA vessel. Right: detail of the inlet/outlet diffuser mesh and its dimensions (mm), and detail of the contact surfaces among the various materials (h_c is the convective heat transfer coefficient).

Fig. 3. Validation of the CFD model. Evolution of the water temperature in the TC, determined experimentally and estimated from the selected and verificated CFD model (S-VA) during the full charge period (107%) and part of the subsequent standby period, until 7,200 s.

Fig. 4. Comparison of the three inner tank wall lining materials: STEEL, PMMA and EPS. Evolution of the water temperature in the TC during the full charge period (107.2%).

Fig. 5. Comparison of the three inner tank wall lining materials. Evolution of the water temperature in the TC during the partial charge (63.8 %, 1,800 s) and the subsequent standby period until 25,200 s.

Fig. 6. Increment of energy accumulated (ΔE), expressed as a percentage of the energy accumulated in relation to that in the adiabatic process (S-AD), in the water domain and in the tank wall for the three inner lining materials. Partial charge (1,800 s, 63.8%) and standby period until 25,200 s.

Fig. 7. Moment of energy (ME) for the three inner lining materials in relation to that in the adiabatic process (S-AD) during the partial charge (1,800 s, 63.8%) and the standby period until 25,200 s.

Fig. 8. Relationship of the conductivity of the inner lining material (STEEL, PMMA, EPS) with the increment of accumulated energy, expressed as a percentage in relation to the adiabatic process at different times.

Fig. 9. Details of the distribution of temperatures (K) for the three inner lining materials at 450 and 2,250 s after the full charge process begins. Y and Z are expressed in m.

Fig. 10. Horizontal temperature profiles at various heights (Z) for the three inner lining materials during the standby period at 3,600 s after the partial charge (1,800 s, 63.8%). Y and Z expressed in m.

Fig. 11. Temperature contours and streamtraces at the end of the partial charge (1,800 s, 63.8%) for the three inner lining materials and the adiabatic case (AD).

Fig. 12. Temperature contours and streamtraces at the end of the standby period (25,200 s) after the partial charge period (1,800 s, 63.8%) for the three inner lining materials and the adiabatic case (AD).

Fig. 13. Streamtraces over the velocity contours and temperature profiles during the standby period after the partial charge (1,800 s, 63.8%) for the three inner lining materials. The ascending velocities zones are depicted in red, while the descending velocities ones are shown in blue. Y and Z are expressed in m.

Fig. 14. Profiles of the vertical velocity of water in the different horizontal planes at time t = 3,600 s during the standby period after the partial charge (63.8%) for the three inner lining materials and the adiabatic case (AD). Y and Z are expressed in m; Velocity Z is expressed in $m \cdot s^{-1}$.

LIST OF TABLE CAPTIONS

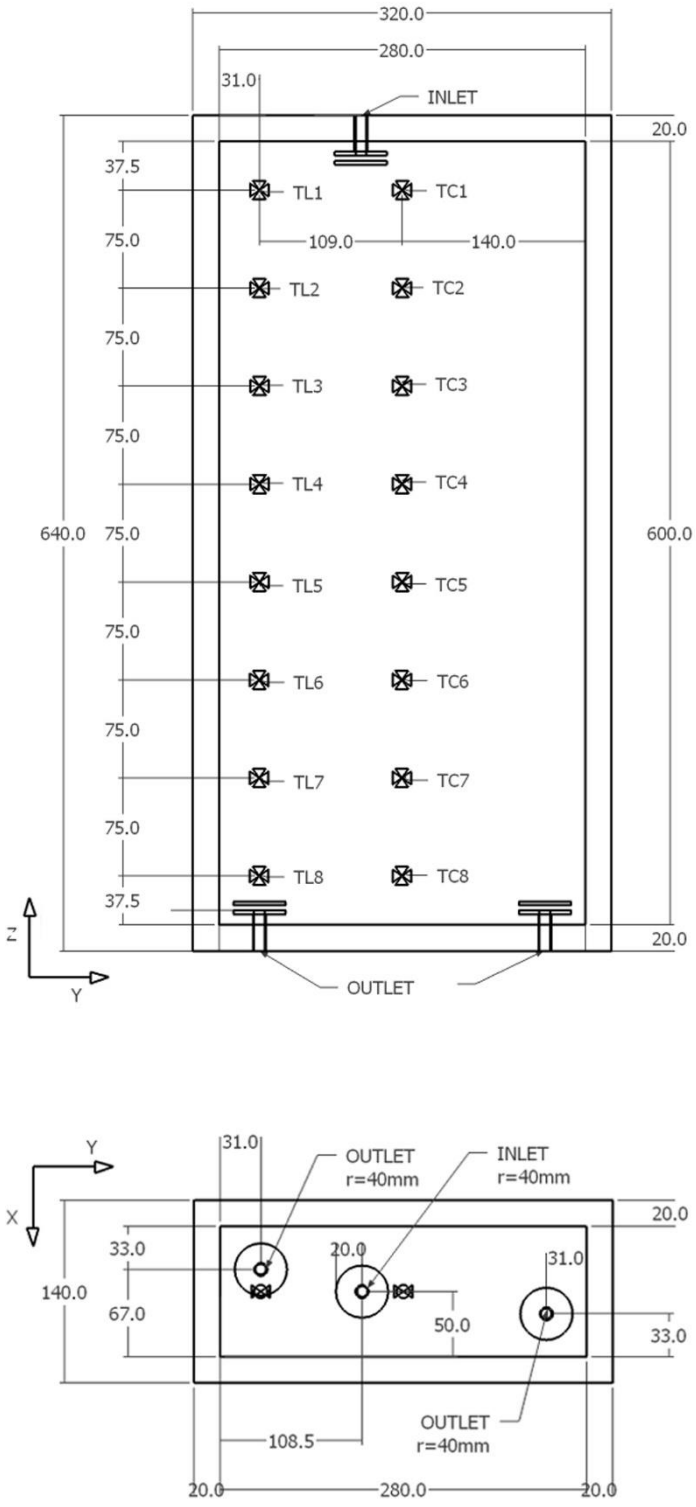

Fig. 1. Schematic view of the tank with its dimensions (mm). The position of the central (TC) and lateral (TL) probes with 8 thermocouples each is also indicated.

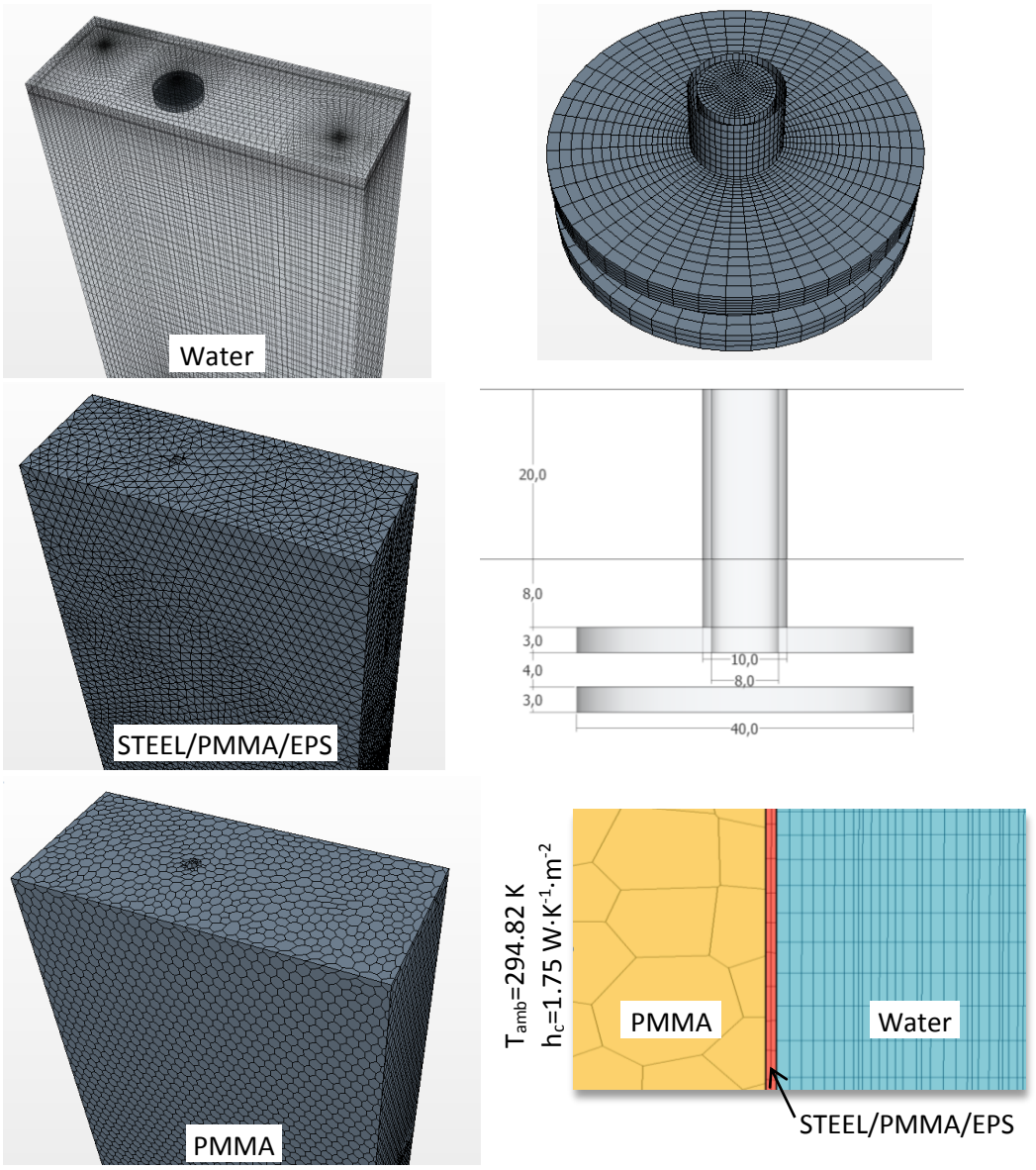

Fig. 2. Left: details of the meshes in the different regions: water, STEEL/PMMA/EPS, and PMMA vessel. Right: detail of the inlet/outlet diffuser mesh and its dimensions (mm), and detail of the contact surfaces among the various materials (hc is the convective heat transfer coefficient).

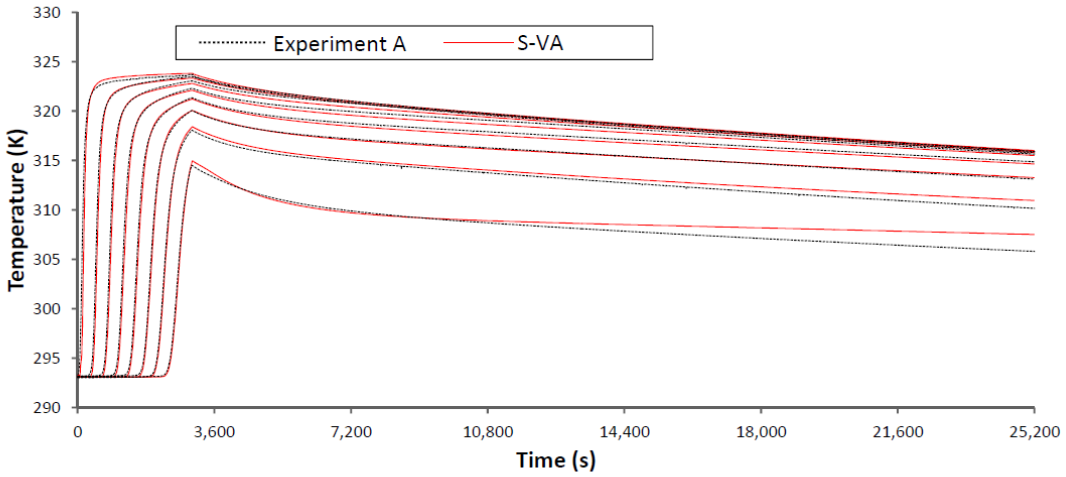

Fig. 3. Validation of the CFD model. Evolution of the water temperature in the TC, determined experimentally and estimated from the selected and verificated CFD model (S-VA) during the full charge period (107%) and part of the subsequent standby period, until 7,200 s.

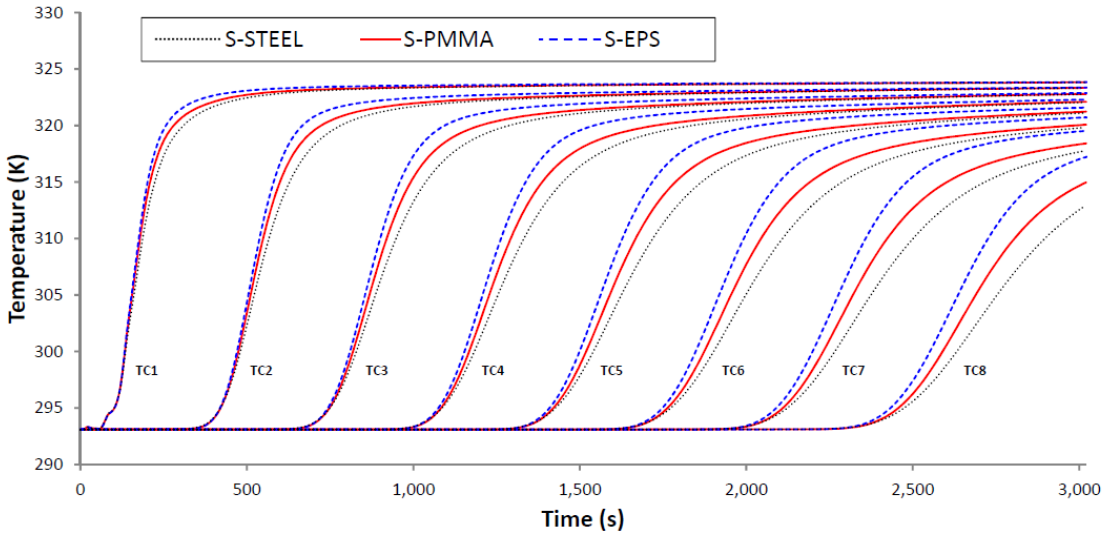

Fig. 4. Comparison of the three inner tank wall lining materials: STEEL, PMMA and EPS.

Evolution of the water temperature in the TC during the full charge period (107.2%).

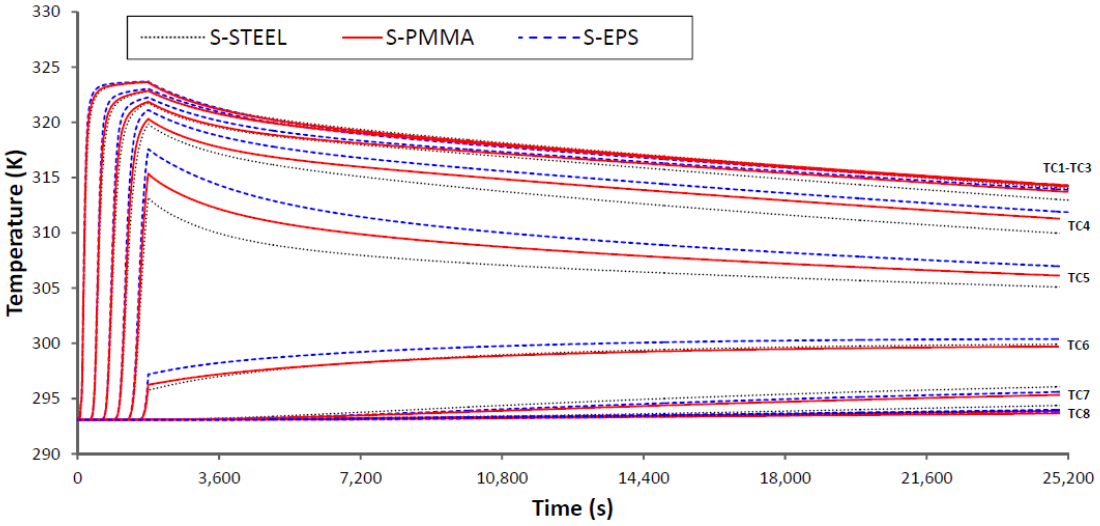

Fig. 5. Comparison of the three inner tank wall lining materials. Evolution of the water temperature in the TC during the partial charge (63.8 %, 1,800 s) and the subsequent standby period until 25,200 s.

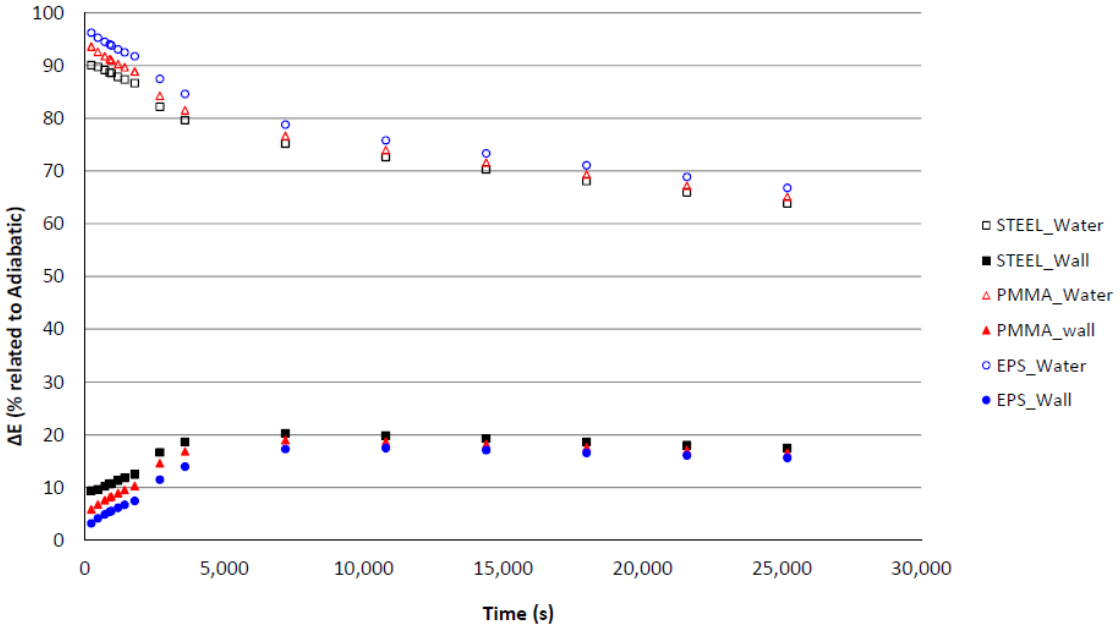

Fig. 6. Increment of energy accumulated (ΔE), expressed as a percentage of the energy accumulated in relation to that in the adiabatic process (S-AD), in the water domain and in the tank wall for the three inner lining materials. Partial charge (1,800 s, 63.8%) and standby period until 25,200 s.

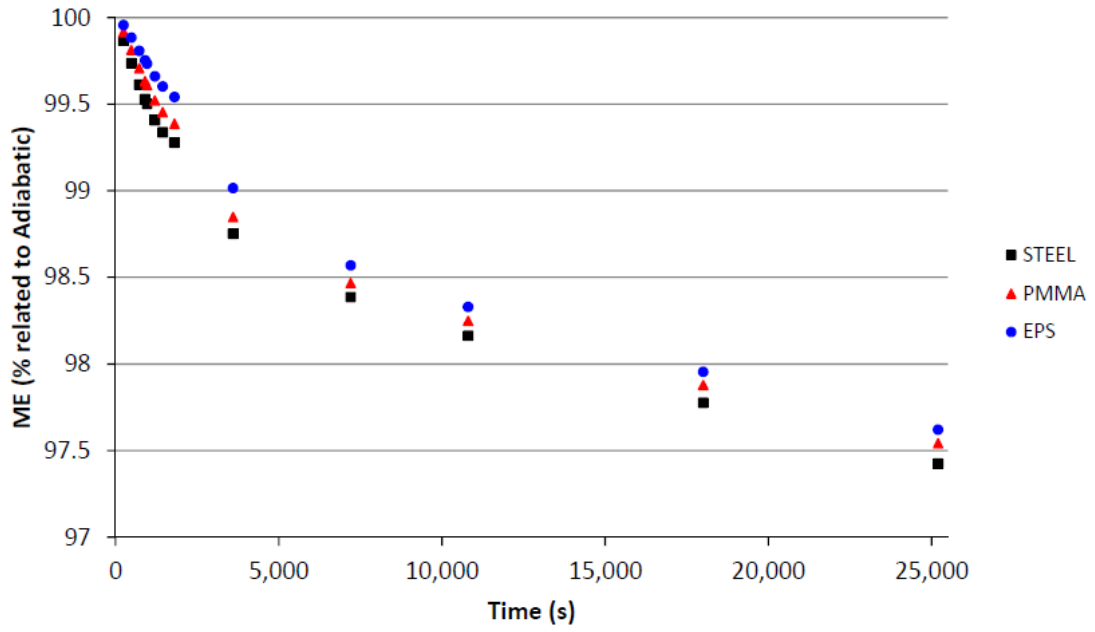

Fig. 7. Moment of energy (ME) for the three inner lining materials in relation to that in the adiabatic process (S-AD) during the partial charge (1,800 s, 63.8%) and the standby period until 25,200 s.

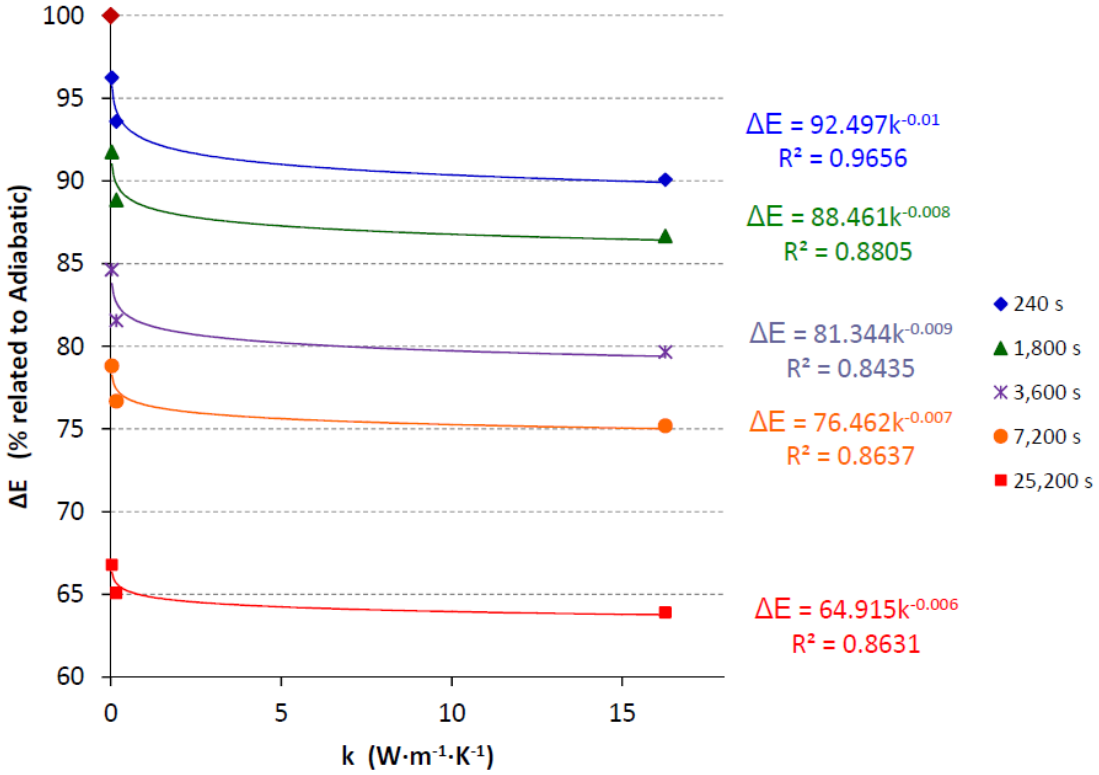

Fig. 8. Relationship of the conductivity of the inner lining material (STEEL, PMMA, EPS) with the increment of accumulated energy, expressed as a percentage in relation to the adiabatic process at different times.

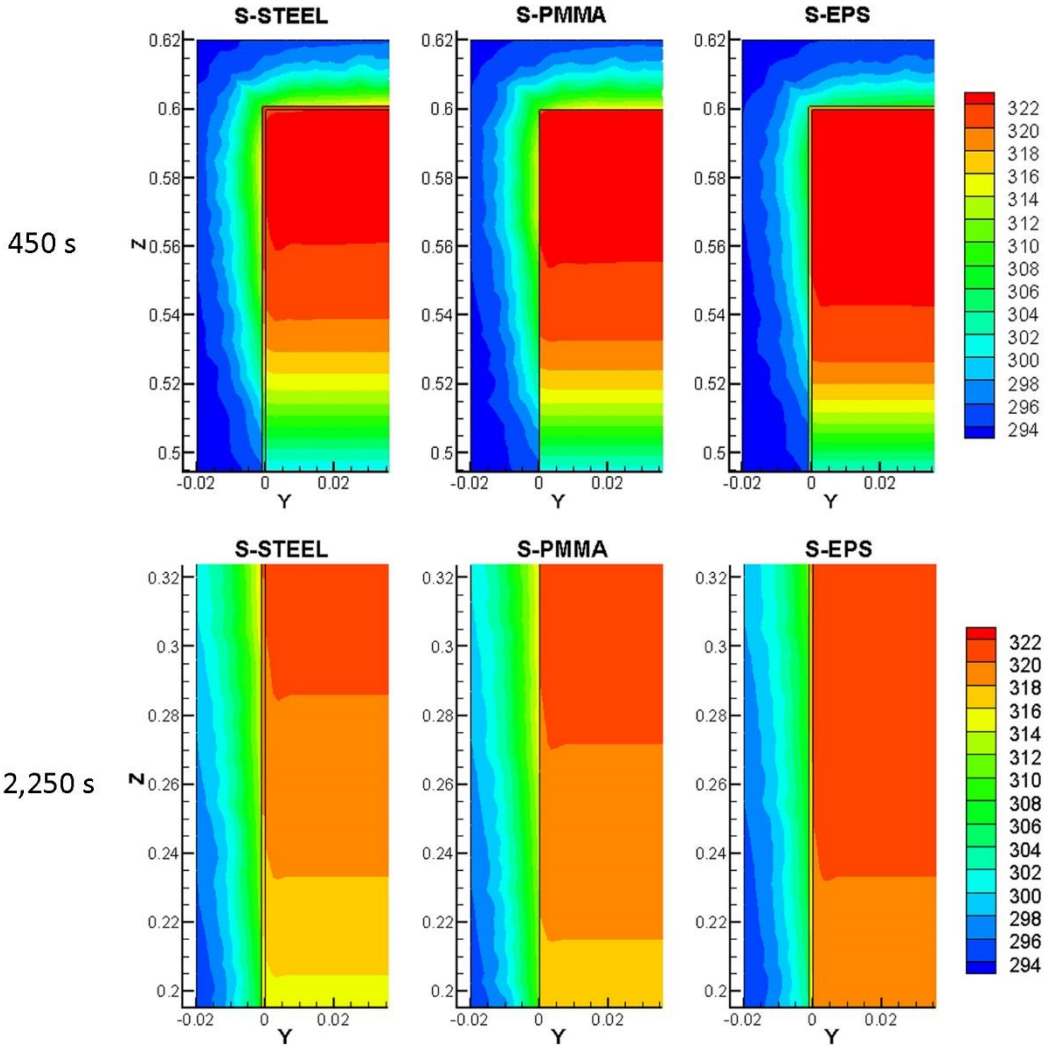

Fig. 9. Details of the distribution of temperatures (K) for the three inner lining materials at 450 and 2,250 s after the full charge process begins. Y and Z are expressed in m.

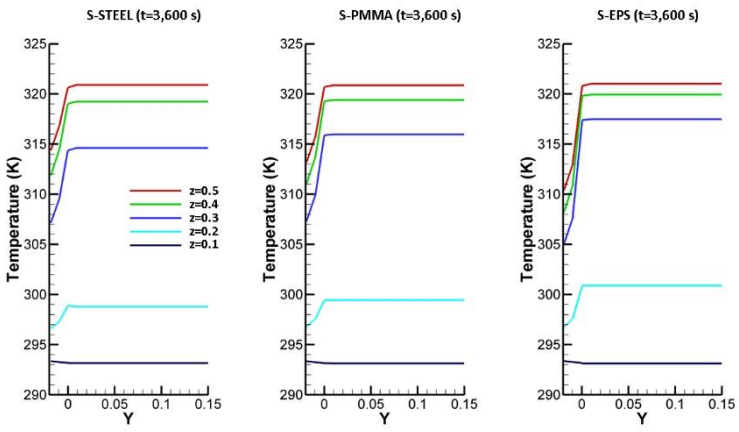

Fig. 10. Horizontal temperature profiles at various heights (Z) for the three inner lining materials during the standby period at 3,600 s after the partial charge (1,800 s, 63.8%). Y and Z expressed in m.

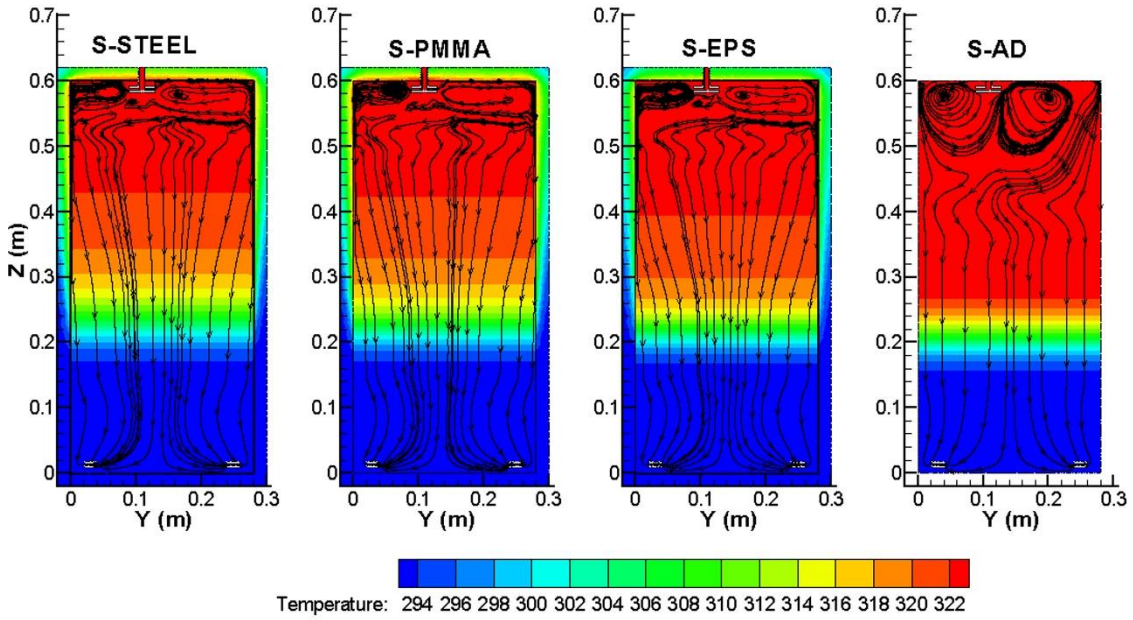

Fig. 11. Temperature contours and streamtraces at the end of the partial charge (1,800 s, 63.8%) for the three inner lining materials and the adiabatic case (AD).

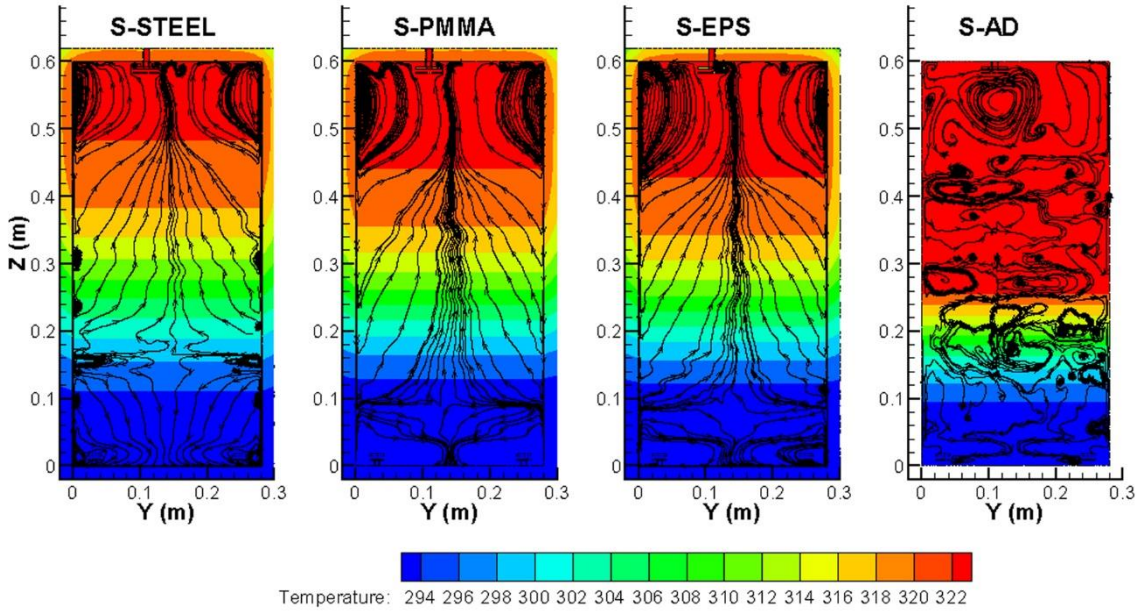

Fig. 12. Temperature contours and streamtraces at the end of the standby period (25,200 s) after the partial charge period (1,800 s, 63.8%) for the three inner lining materials and the adiabatic case (AD).

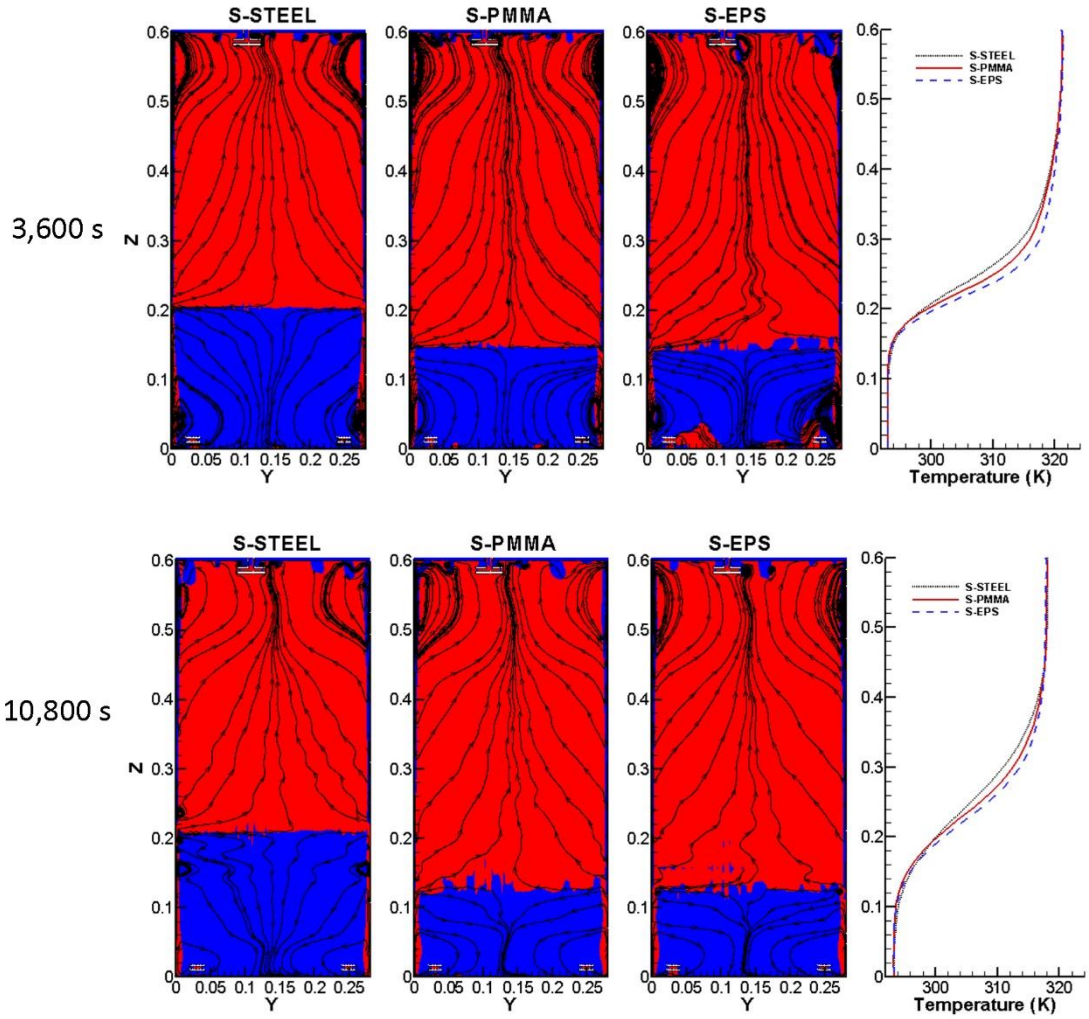

Fig. 13. Streamtraces over the velocity contours and temperature profiles during the standby period after the partial charge (1,800 s, 63.8%) for the three inner lining materials. The ascending velocities zones are depicted in red, while the descending velocities ones are shown in blue. Y and Z are expressed in m.

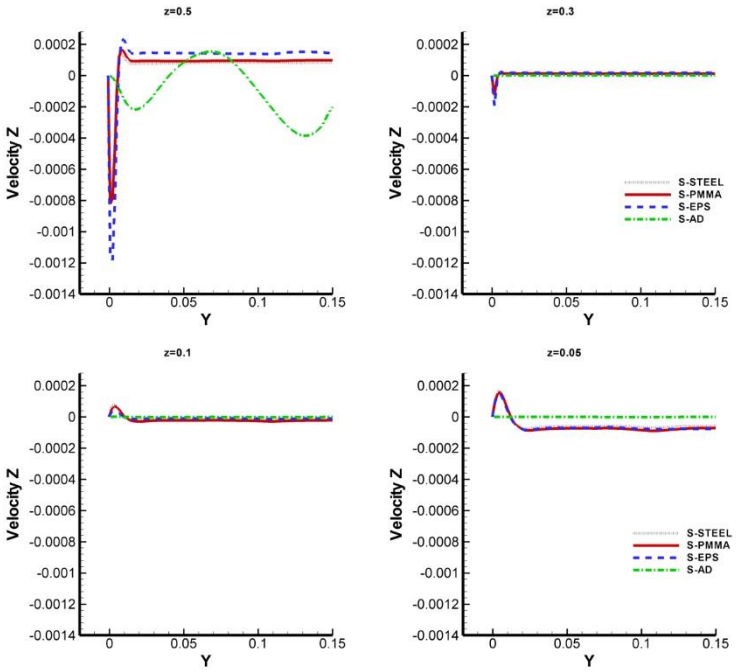

Fig. 14. Profiles of the vertical velocity of water in the different horizontal planes at time t = 3,600 s during the standby period after the partial charge (63.8%) for the three inner lining materials and the adiabatic case (AD). Y and Z are expressed in m; Velocity Z is expressed in m·s-1.

Table 1. Experimental trials used to develop the CFD model.

Experimental trials (simulation case)	Duration of charge (s)	Renovation of stored water (%)	T_{inlet} (K)	Q ($mL \cdot s^{-1}$)	T_{ini} (K)	T_{amb} (K)	Duration of Standby period (s)
A (S-VA)	3,022.2	107	324.08	6.0	293.08	294.82	25,200
B (S-VB)	1,309.7	117	324.62	15.0	293.23	294.48	25,200

T_{inlet} (K): Mean hot water inlet temperature during the charge.
Q ($mL \cdot s^{-1}$): Water flow injected and extracted during the charge.
T_{ini} (K): Mean initial water temperature.
T_{amb} (K): Ambient temperature.

Table 2. Cell characteristics of the water domain mesh. SE: Shortest Edge; LE: Longest Edge.

Type mesh	SEx (mm)	LEx (mm)	SEy (mm)	LEy (mm)	SEz (mm)	LEz (mm)	Number of Grid Points
A	6.8	11	5.7	11.7	2	14.8	300,000
B	6.8	11	5.7	11.7	0.7	9.2	480,000
C	5.5	5.7	5.7	5.9	0.7	9.2	900,000

Table 3. Cases analyzed to study the influence of inner tank lining material on stratification.

Case	Inner tank wall lining material	Tank wall material and insulation	Observations
S-PMMA (S-VA)	1 mm PMMA $k_{(PMMA)} = 0.16\ W \cdot m^{-1} \cdot K^{-1}$	19 mm PMMA + 20 mm IM	Experimental model. Intermediate thermal conductivity
S-STEEL	1 mm STEEL $k_{(STEEL)} = 16.26\ W \cdot m^{-1} \cdot K^{-1}$	19 mm PMMA + 20 mm IM	Lining with high thermal conductivity
S-EPS	1 mm EPS $k_{(EPS)} = 0.034\ W \cdot m^{-1} \cdot K^{-1}$	19 mm PMMA + 20 mm IM	Lining with low thermal conductivity
S-AD	Not considered	Not considered	Adiabatic model

IM: Insulating Material (flexible elastomeric foam).